J. Fluid Mech. (1995), *vol.* 296, *pp.* 185–209

On turbulent spots in a laminar boundary layer subjected to a self-similar adverse pressure gradient

By AVI SEIFERT AND ISRAEL J. WYGNANSKI

Department of Fluid Mechanics and Heat Transfer, Faculty of Engineering, Tel-Aviv University, Ramat-Aviv 69978, Israel

(Received 10 June 1994 and in revised form 4 March 1995)

The characteristics of a turbulent spot propagating in a laminar boundary layer subjected to a self-similar adverse pressure gradient (defined by a Falkner–Skan parameter $\beta = -0.1$) were investigated experimentally. It was observed that some small differences in the normalized shape of the undisturbed velocity profile caused by the pressure gradient had a major influence on the spreading rate of the spot at comparable Re_{δ^*}. The rate of spread of the spot in the spanwise direction was affected most dramatically by the pressure gradient where the average angle at which the tips of the spots moved outward relative to the plane of symmetry was 21°. It was noted that the strength and duration of the disturbance initiating the spots had an effect on their spanwise rate of spread. For example, a strong impulsive disturbance and a disturbance caused by a stationary three-dimensional roughness generated spots which spread at a much smaller rate. The interaction of the spot with the wave packet existing beyond its tip was enhanced by the adverse pressure gradient because the Reynolds number of the surrounding boundary layer was everywhere supercritical. Thus, the maximum linear amplification rate in this case is approximately four times larger than in Blasius flow. Some features of the breakdown and their relationship to the shape and the perturbation velocities in the spot are discussed. The normalized length of the calmed region relative to the length of the spot is enhanced by the adverse pressure gradient and by an increase in the intensity of the disturbance.

1. Introduction

The propagation of a turbulent spot in a laminar boundary layer has been studied extensively because the spot represents the final stages of a natural transition process (e.g. Emmons 1951; Narasimha 1985). It is known that the evolution of spots generated by an impulsive disturbance is independent of the type of perturbation initiating them (Wygnanski, Sokolov & Friedman 1976) while experiments relying on flow visualization suggested that naturally occurring spots are identical to those generated by impulsive perturbation. It became standard practice, therefore, to investigate artificially generated spots (e.g. Gostelow *et al.* 1993). Most spot studies were carried out in the absence of a pressure gradient and, thus, relatively little is known about the effect of a pressure gradient on the rate at which laminar flow is contaminated by turbulence. Empirical correlations are used to model the last stages of the transition and the concomitant rise in skin friction. Detailed knowledge of the spot's behaviour will not only substantiate and improve such models but will also help us to understand the mechanisms of the transition process. A pressure gradient affects

the stability of the laminar boundary layer (Wazzan, Okamura & Smith 1968) because it alters the shape of the velocity profile, which, in turn, serves as a parameter in the Orr–Sommerfeld equation. The role of the pressure gradient in a bypass-transition process (Morkovin 1969) initiated by a strong disturbance or large-scale roughness is not well understood.

There are some comparative studies of the effects of pressure gradients on the propagation and growth of the spot. Katz, Seifert & Wygnanski (1990) observed a reduction in the rate of spread of the spot in a highly favourable pressure gradient, while Gostelow *et al.* (1993) observed an accelerated destabilization of the flow in an adverse pressure gradient. The spanwise spreading rate of the spot was linked with the linear stability model when Wygnanski, Haritonidis & Kaplan (1979) observed two inclined wave packets trailing from the tips of the spot in a Blasius boundary layer. Waves appeared to have been absent in the investigation of Cantwell, Coles & Dimotakis (1978) owing to the favourable pressure gradients that existed in their experiment (equivalent to a Falkner–Skan parameter $\beta = 0.25$). Waves were observed by Chambers & Thomas (1983), but they were considered as 'passive attendants' to the spot (i.e. they simply trailed the spot), partly because of the subcritical Reynolds number in which these experiments were carried out. Glezer, Katz & Wygnanski (1989) realized that the waves originated from a perturbed region travelling with the tip of the spot. When the Reynolds number based on the laminar boundary layer parameters was supercritical, these waves amplified and broke down, creating a separate turbulent region that, in time, joined the spot. This process distorts the trailing edge of the spot, giving it a characteristic arrow-head shape. A spot developing in a favourable pressure gradient (i.e. at $\beta = 1$, Katz *et al.* 1990) did so at a highly subcritical Reynolds number and, therefore, was not accompanied by secondary breakdown. In fact no waves were observed in this case, and the trailing edge of the spot was straight and perpendicular to the direction of streaming. The spanwise rate of spread of the spot in a favourable pressure gradient was approximately 50% of the spanwise spreading rate in a Blasius boundary layer at comparable Reynolds numbers (i.e. the included half-angle was only about 5° at $\beta = 1$ in comparison to 10° at $\beta = 0$). Thus the suggested 'growth by a destabilization' process (Gad-el-Hak, Blackwelder & Riley 1981) was weakened by the favourable pressure gradient. The fact that the spot continues to spread in spite of the highly stable surroundings may be attributed to the spanwise velocity that exists within the turbulent region and pushes the turbulent fluid outward (Seifert, Zilberman & Wygnanski, 1994). There is no information about the effect of a pressure gradient on the spanwise velocity component in and around the spot. Gostelow *et al.* (1993) observed the existence of high-amplitude waves near the spot evolving in an adverse pressure gradient, but they did not chart their characteristics. Furthermore, they observed that the spanwise rate of spread of their spot was almost twice as rapid as the spot evolving in a Blasius boundary layer.

The purpose of the present investigation is to study the evolution of a turbulent spot in a self-similar laminar boundary layer subjected to an adverse pressure gradient having a Falkner–Skan parameter $\beta = -0.1$. The self-similarity is important because it reduces the number of parameters governing this complex problem. For example, the strength and the duration of the perturbations generating the spots were altered in order to assess their importance on the overall characteristics of the spot. An effort is made to compare quantitatively the spot characteristics measured here to past investigations carried out in a laminar boundary layer at $\beta = 0$ and $\beta = 1$. For this purpose all experimental procedures and data reduction criteria are as close as possible to the ones used previously.

2. The experiment

The experiment was conducted in the closed-loop low-turbulence wind tunnel located at Tel-Aviv University (see Wygnanski *et al.* 1976 for a detailed description of the facility). The experimental methodology used was developed in earlier studies by Glezer *et al.* (1989) and Katz *et al.* (1990). The tunnel was refurbished in 1988 (seamless stainless steel screens were installed, and the contraction section was modified internally by fitting a longer fifth-order polynomial to the external contour), which resulted in some reduction of the turbulence level and thinner wall boundary layers. The present RMS level of the u' fluctuations in the test section is less than 0.03%, with the plate, its flap, and the traversing mechanism installed in the tunnel. The entire experiment was automated (Seifert 1990). The tunnel speed, the hot-wire calibration procedure, and the traversing mechanism, in all of its three directions, were controlled by a computer and could be activated from a remote site. The programs activating the probe-traverse and the data acquisition were coupled and could automatically select incremental distances from the surface depending on the measured velocity and its local gradient.

The measurements were carried out on a flat polished aluminium plate 19 mm thick and 2.5 m long which was installed vertically in the 6 m long test section. The adverse pressure gradient was generated by a flexible, Plexiglas insert anchored to the test-section wall, opposite to the flat plate on which the measurements were carried out (figure 1). The pressure gradient was adjusted by changing the contour of this surface through adjustable screw-jacks located in the gap between the sidewall and insert. This arrangement provided the designed pressure gradient, without the concomitant presence of surface curvature, and thus enabled the separation of the two effects. The plate has a fairly blunt (3:1 axes ratio) elliptic leading edge. It has also a trailing-edge flap, which was used to control the circulation around the entire plate, thus altering the location of the leading-edge stagnation line. Most of the secondary flow, originating at the juncture of the plate and the tunnel walls, was forced to bleed to the rearward side of the plate through adjustable slots. This was achieved by slightly increasing the static pressure on the working side of the plate, relative to the rearward side, with a screen located at the trailing edge of the plate. The suction slots and the screen helped to maintain a long fetch of laminar flow on that surface, delaying the initialization of transition to a Reynolds number of $0.5\text{–}0.6 \times 10^6$. This was the Re_x at which intermittency was first observed 1200 mm downstream of the leading edge of the plate at the prescribed pressure gradient and a reference velocity of 7.2 m s^{-1}. The free-stream velocity measured by a Pitot–Prandtl tube located 23 cm downstream of the leading edge (figure 1) was maintained at 6, 7.5 and 9 m s^{-1}, respectively, throughout each experiment.

Controlled disturbances were generated either by miniature earphones (used commercially for hearing aids) embedded in the rear surface of the flat plate or by compressed air passing through a solenoid valve. Both actuators ejected puffs of air through a 0.5 mm orifice located either 30 or 50 cm from the leading edge of the plate. Most of the data were acquired when the spot originated at $X_p = 50$ cm, because downstream of this location the flow was self-similar. The free-stream velocities at this location were approximately 5% lower than at the location of the Pitot tube (i.e. they were maintained at either 5.8, 7.2 or 8.6 m s^{-1}, respectively). Some data was taken when the disturbance source was located at $X_p = 30$ cm because it provided a longer fetch before the spot interacted with turbulent regions occurring naturally in the flow. The two streamwise locations at which the spot originated and the three free-stream

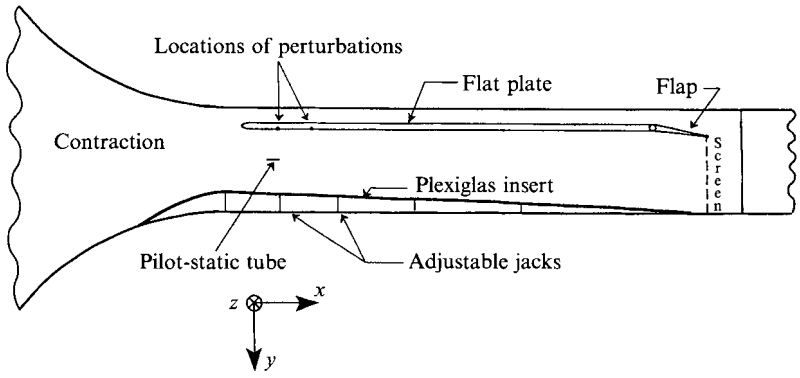

FIGURE 1. A schematic sketch of the experimental setup.

reference velocities enabled us to assess the effect of Reynolds number on the spot evolving in an adverse pressure gradient.

The injection velocity was estimated to be of the same order as that of the free stream. The duration of the impulse was between 3–5 ms when an earphone was used, and it was approximately twice as long when the compressed air was used. The difference in the injection velocity and the duration of the perturbation enabled us to assess, at least partly, the effect of the source strength and its duration on the development of the spot.

3. Discussion of results

3.1. *The base flow*

The evolution of a spot is well documented for a boundary layer in the absence of a pressure gradient. More recently the spot was mapped in the presence of a strong favourable pressure gradient corresponding to the flow prevailing near a front stagnation point (Katz *et al.* 1990). One of the purposes of these studies was to provide a database that would link the characteristic features of the spot with the stability of the surrounding laminar boundary layer. The present investigation provides such data when the spot evolves in a self-similar boundary layer subjected to an adverse pressure gradient that is described by the Falkner–Skan parameter $\beta = -0.1$. In the absence of a pressure gradient (i.e. for $\beta = 0$), the boundary layer thickness increases in the direction of streaming, as the square root of the distance from the leading edge and the velocity of the free stream are constant. Near a stagnation point ($\beta = 1$), the velocity outside the boundary layer is proportional to the distance measured from the stagnation location, and the thickness of the boundary layer is constant. The Reynolds number based on the local velocity and thickness of the boundary layer is proportional to $X^{1/2}$ for $\beta = 0$ and to X for $\beta = 1$, yet the boundary layer developing near the stagnation location is much more stable than the boundary layer evolving in the absence of a pressure gradient because of the shape of its normalized velocity profile.

Although the adverse pressure gradient corresponding to $\beta = -0.1$ is fairly weak, as it is distant from the condition at which laminar separation occurs (i.e. at $\beta = -0.1988$), it has a major effect on the linear stability of the boundary layer because it contains an inflection point in the flow at around $Y/\delta^* = 0.75$, where the local velocity is 40% of the free-stream velocity. All the measurements were made on a flat surface in order to ensure that the instabilities observed will not be affected by the curvature of the streamlines (i.e. that the flow will not be influenced by centrifugal

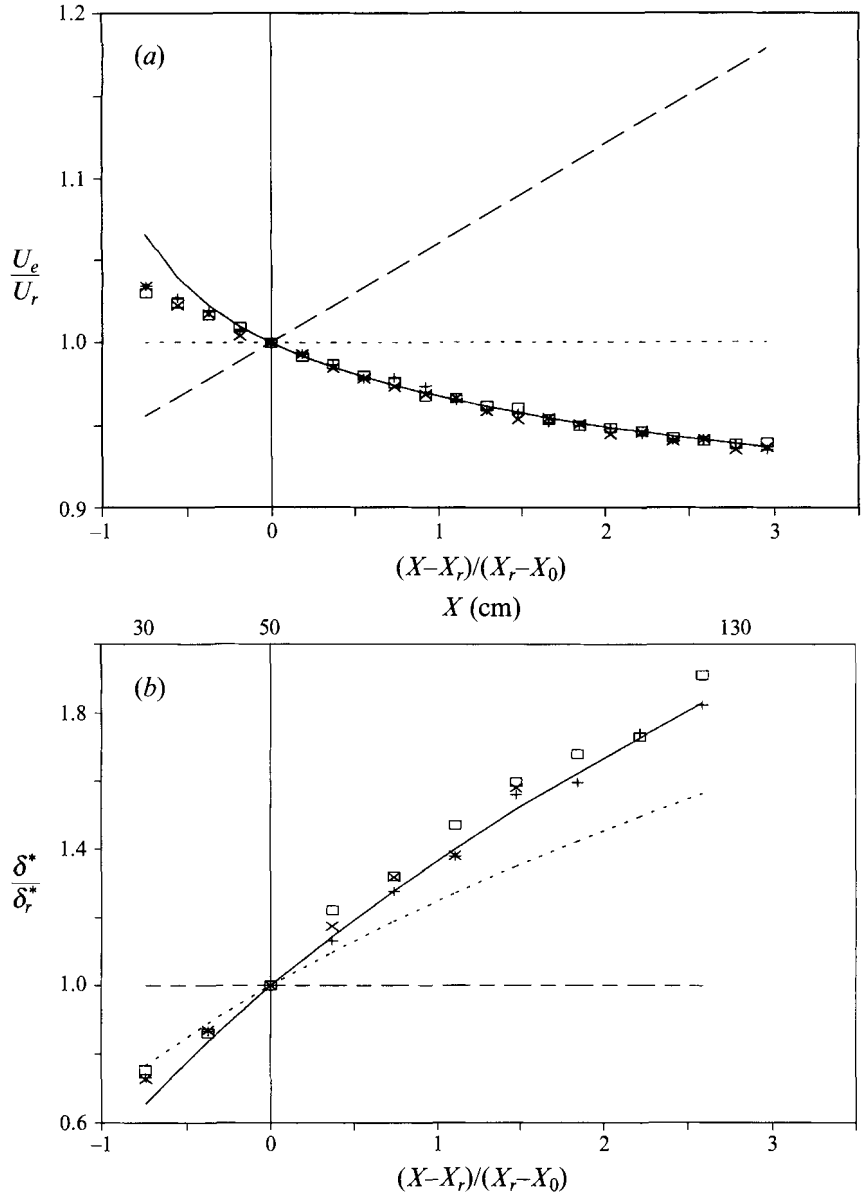

FIGURE 2. (*a*) The variation of the free-stream velocity with X. (*b*) The displacement thickness of the unperturbed laminar boundary layer. □, $U_r = 5.8$ m s^{-1}; +, 7.2 m s^{-1}; ×, 8.6 m s^{-1}; ——, theory; ---, $\beta = 0$; ———, $\beta = 1$. $X_0 = 23$ cm in (*a*) and 12 cm in (*b*) (theory).

forces as analysed by Görtler (see the recent review by Saric 1994). The pressure gradient was therefore generated by a contoured insert, which was placed on the opposite wall of the wind tunnel and changed the area of the test section in the direction of streaming (figure 1). The free-stream velocity outside the boundary layer and the displacement thickness of the boundary layer should vary as

$$U_e \propto (X-X_0)^{\beta/(2-\beta)} \quad \text{and} \quad \delta^* \propto (X-X_0)^{(1-\beta)/(2-\beta)}, \tag{1}$$

where X_0 is the virtual origin of the flow, which depends on the shape of the leading edge of the plate and on the manner in which the pressure gradient was generated; it

may also depend on Reynolds number, although to a weaker extent. One may also note that the virtual origin fitting the self-similar lengthscale may be different from the X_0 derived for the velocity scale. A constant reference velocity, U_r, and lengthscale, δ_r^*, were so chosen as to coincide with the location at which β achieved the desired value of -0.1, and the disturbance initiating the turbulent spot was also, though not always, placed at this location (i.e. at $X_p = X_r = 50$ cm from the plate's leading edge). The variation of the dimensionless velocity (U_e/U_r) in the direction of streaming outside the boundary layer was measured for three reference velocities, 5.8, 7.2 and 8.6 m s^{-1}, and is plotted in figure 2(*a*). The theoretical curve represented by (1) yields $U_e \propto (X-X_0)^{-0.0476}$ and is marked by a solid line on this plot, demonstrating a good agreement between the measurements and theory. The dashed and dotted lines represent the values for $\beta = 1$ (Katz *et al.* 1990) and $\beta = 0$ (Wygnanski *et al.* 1976) used in previous experiments. The location of the virtual origin is dependent on the pressure gradient. It almost coincides with the leading edge of the plate ($X_0 = 3.2$ cm) in the absence of a pressure gradient, it is located at $X_0 = 23$ cm in the present case, while it is at $X_0 = -400$ cm for $\beta = 1$. These numbers do not alter the character of the boundary layer under investigation, but they are indicative of the manner in which the flow was generated. A simulated stagnation flow, extending over a long distance, can only be achieved by converging the tunnel walls and thus moving the virtual origin of the flow far upstream of the leading edge of the plate. In order to compare data measured at different pressure gradients and Reynolds numbers, the streamwise distance from the reference location is normalized by the distance of the reference location from the virtual origin $(X_r - X_0)$. The rate at which the boundary layer thickens with downstream distance is plotted in figure 2(*b*) and compared to experimental observations. The displacement thickness is used throughout this investigation as a characteristic lengthscale representing the thickness of the boundary layer because it is precisely defined and measured with the least ambiguity. The displacement thickness, δ_r^*, for $U_r = 5.8$, 7.2 and 8.6 m s^{-1} measured at $X_r = 50$ cm, was 2, 1.8 and 1.65 mm, respectively, and was used as the reference length. The increase in the theoretically predicted displacement thickness in the direction of streaming is proportional to $(X-X_0)^{0.524}$, and this exponent is also plotted on figure 2(*b*). The rates of spread of the other two boundary layers referred to previously are also plotted in this figure.

The normalized shapes of the laminar velocity profiles for $\beta = 1$, 0 and -0.1 are plotted in figure 3. The symbols, however, refer to the present experiments only. The measured velocity profiles agree well with theory and depict correctly the inflectional character of the profile at streamwise distances exceeding 50 cm from the leading edge. The data taken 30 cm from the leading edge are also plotted to show that, at this streamwise location, the flow is still adjusting to the imposed pressure gradient and the free stream is decelerating at a slower rate than is required for $\beta = -0.1$ (figure 2*a*). The experimental resolution used in setting the pressure gradient and measuring β is ± 0.02. The normalized velocity profile at $X = 30$ cm fits the profile appropriate to the absence of a pressure gradient better (i.e. the Blasius flow) than that appropriate to the chosen β. We have plotted the normalized velocity profile for three values of β in order to emphasize the significance of the small variation in the shape of the profile on the stability of the flow. The differences in the shape of the profile between $\beta = 0$ (dotted curve on figure 3) and $\beta = -0.1$ (solid curve) approach the experimental resolution of conventional velocity measurements. Although the difference in the shape factor, $H = \delta^*/\theta$ (where θ is the momentum thickness) between the two cases, is only 7.5% ($H = 2.59$ for Blasius flow and 2.80 for $\beta = -0.1$), the differences in the stability

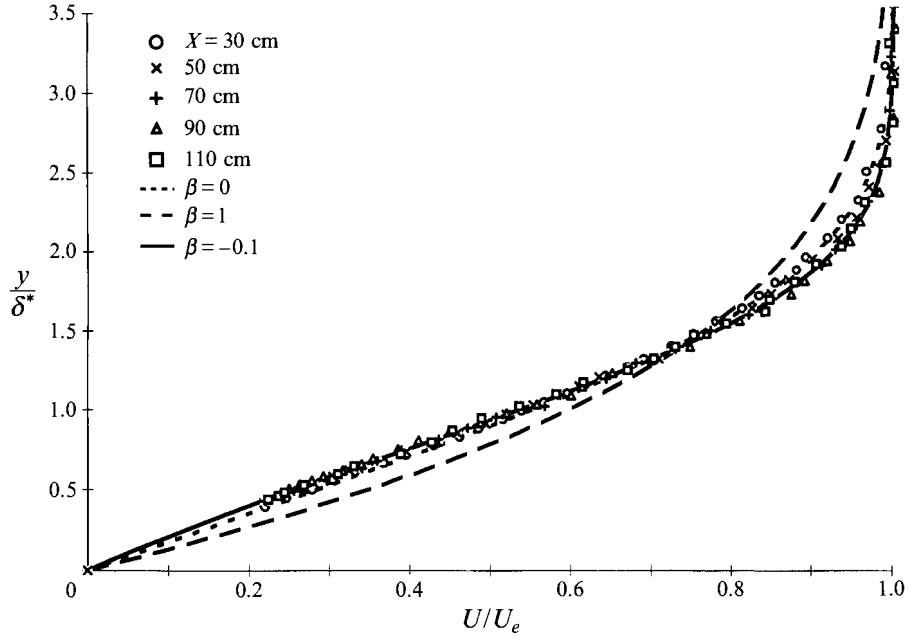

FIGURE 3. The shape of the normalized velocity profiles measured in the present work and compared to Falkner–Skan velocity profiles.

characteristics are significant. For example, the critical Re_{δ^*}, which is 520 for Blasius flow, becomes 200 for $\beta = -0.1$, while the most unstable frequency, $\omega\nu/U_e^2$, near this Re_{δ^*} increases from 2×10^{-4} to 9×10^{-4} and the maximum two-dimensional exponential amplification rate at $Re_{\delta^*} = 900$ increases fourfold. It suffices to mention that the critical Re_{δ^*} corresponding to $\beta = 1$ is 13000!

We are accustomed to comparing the various types of 'Falkner–Skan' velocity profiles when they are plotted against a parameter

$$\eta = \frac{Y}{X}\left[\frac{1}{2-\beta}\left(\frac{U_e X}{\nu}\right)\right]^{1/2}$$

which scales the distance from the surface with the distance from the leading edge and with a local $Re_x^{1/2}$. In these coordinates, the profiles seem to be strongly affected by small variations in β, but this effect is fictitious whenever the Reynolds number is a parameter, and this is certainly the case in stability calculations. One must conclude that small differences in the derivatives of the velocity profile (first derivative when one solves the primitive linearized equations or second derivative if one solves the Orr–Sommerfeld equation) are the most significant factors for a given local Re_{δ^*}. One should remember that a change in the critical value of Re_{δ^*} between $\beta = 0$ and $\beta = -0.1$ implies a change in the ratio of the critical $(X - X_0)$ distances in excess of 6 for identical reference velocities. The significance of this effect should not be underestimated in view of the small differences in the shape of the profiles as shown in figure 3.

3.2. *The effect of* $\mathrm{d}P/\mathrm{d}X$ *on the spot size and spreading rates*

The general shape of a turbulent spot, its rate of spread in the surrounding laminar boundary layer, and the propagation speeds of its boundaries in the absence of a pressure gradient are fairly well documented. The ensemble-averaged boundaries of the

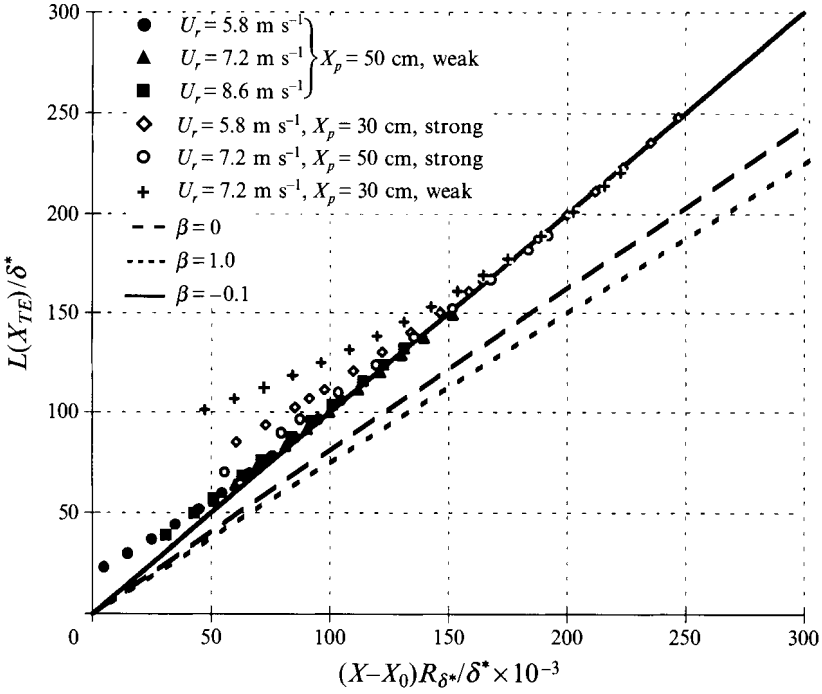

FIGURE 4. The normalized length of the spot based on the trailing-edge's location.

spot can be determined by different criteria. An 'on–off' signal locating the turbulent interface (see Glezer *et al.* 1989 for a detailed description) is one such criterion, and the location at which the intermittency factor γ is 50% (i.e. in 50% of the events the hot wire at the prescribed location recorded a turbulent flow while in the other 50% of the events the flow was laminar) represents the average location of the spot's boundary at any given time. Whenever $\gamma > 50\%$, the region is considered turbulent and included within the average boundaries of the spot, although there were realizations in which the boundaries were different. In early experiments, velocity perturbation contours representing $(U-U_{Lam.})/U_e = -0.02$ were also used to mark a hypothetical mean boundary of the spot; the differences between these two definitions are small everywhere except in the immediate vicinity of the solid surface (see Wygnanski *et al.* 1976). It is well known (Schubauer & Klebanoff 1956; Cantwell *et al.* 1978; Wygnanski, Zilberman & Haritonidis 1982) that the streamwise length of the spot, L_x, along its plane of symmetry is approximately proportional to the distance from its origin and, therefore, the rate of elongation, $\mathrm{d}L_x/\mathrm{d}X$, is a constant. It was observed (see Wygnanski *et al.* 1982, figure 14) that $\mathrm{d}L_x/\mathrm{d}X$ is not a universal constant, but depends on the character of the boundary layer at the origin of the spot. Thus the Reynolds number based on δ^* at the source, $(Re_{\delta^*})_p$, was selected as the leading parameter describing the character of the surrounding boundary layer near the origin of the spot. It turned out (Wygnanski *et al.* 1982) that, in the absence of a pressure gradient, $\mathrm{d}L_x/\mathrm{d}X \propto (Re_{\delta^*})_p$ in the range of $(Re_{\delta^*})_p$ considered. Katz *et al.* (1990) also observed that $L_x \propto (Re_{\delta^*})_p \times (X-X_p)$, in spite of the strongly favourable $\mathrm{d}P/\mathrm{d}X$ in their experiment. The same correlation is also valid in the present experiment (figure 4).

The data plotted in figure 4 were shifted in X before being normalized in order to correlate L_x with the virtual origin of the spot, X_0, rather than the disturbance location,

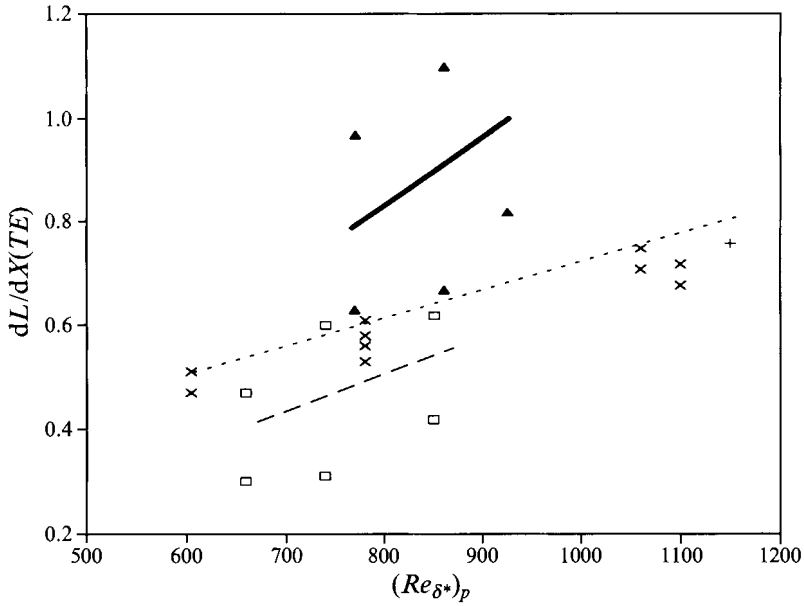

FIGURE 5. Spot's elongation rate with respect to the Reynolds number at the source: ×, ---, $\beta = 0$ (Wygnanski *et al.* 1982); +, $\beta = 0$ (Schubauer & Klebanoff 1956); □, ——, $\beta = 1$ (Katz *et al.* 1990); ▲, ——, $\beta = -0.1$.

X_p. The streamwise distances used in figure 4 refer to the location of the *trailing edge* of the spot, as done by Wygnanski *et al.* (1982), rather than the leading edge, as reported by Katz *et al.* (1990). Therefore the data of Katz *et al.* were reprocessed to determine L_x and $\mathrm{d}L_x/\mathrm{d}X$ at the streamwise location of the spot's trailing edge. The filled symbols shown in figure 4 represent spots generated in the self-similar boundary layer (i.e. at $X_p = 50$ cm) using an impulsive but weak disturbance. These data collapse quickly onto a single curve. Spots generated by a strong disturbance at the same location collapse only at $10^{-3} \times (X - X_0)\, R_{\delta^*}/\delta^* > 130$. Spots generated upstream of the self-similar boundary layer (i.e. at $X_p = 30$ cm) join the asymptotic length curve at $10^{-3} \times (X - X_0)\, R_{\delta^*}/\delta^* = 180$. The streamwise distances at which measurements were carried out were short because the flow underwent natural transition at $Re_x > 5 \times 10^5$, corresponding to a distance of 600–800 mm downstream of the location at which the boundary layer became self-similar and approximately 1100–1300 mm from the leading edge. Thus the relation $L_x \propto (Re_{\delta^*})_p \times (X - X_0)$, which was found first to be valid for the 'stagnation-flow' boundary layer in which δ^* did not vary with X, is also reasonably valid for the *asymptotic* length of the spot at $\beta = -0.1$. The comparison with other spot lengths (figure 4) suggests that the normalized length of the spot has been increased by the adverse pressure gradient.

The rates of elongation of the spots ($\mathrm{d}L_x/\mathrm{d}X$) at the three pressure gradients mentioned earlier are plotted in figure 5. For $\beta = 0$, $\mathrm{d}L_x/\mathrm{d}X$ is a constant dependent only on the Reynolds number prevailing at the perturbation, $(Re_{\delta^*})_p$. At other pressure gradients, $\mathrm{d}L_x/\mathrm{d}X$ is not exactly a constant. The general dependence of $\mathrm{d}L_x/\mathrm{d}X$ on the pressure gradient is clearer than the dependence of L_x on X since these data are independent of the virtual origins and thus less sensitive to the strength and type of the perturbation. One may conclude that the rate of elongation of the spot is increased by approximately 50% by the adverse pressure gradient at comparable $(Re_{\delta^*})_p$.

The influence of a pressure gradient on the celerity of the spot's trailing interface is

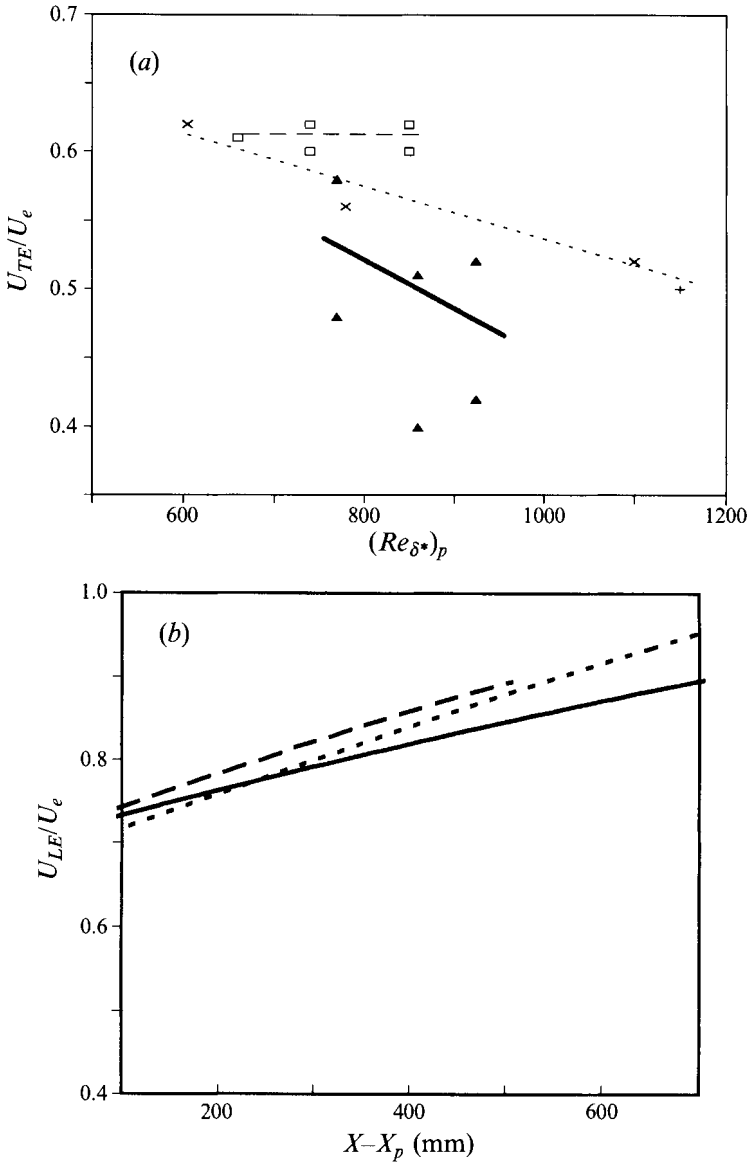

FIGURE 6. The convection velocity of the spot interfaces: (*a*) trailing interface (for symbols see figure 5), (*b*) leading interface, $\beta = -0.1$, $Z_p = 4$ cm, $X_p = 50$ cm: ——, $U_r = 5.8$ m s^{-1}; ---, 7.2 m s^{-1}; – – –, 8.6 m s^{-1}.

plotted in figure 6(*a*) as a function of $(Re_{\delta^*})_p$. In the absence of a pressure gradient, this quantity scales with the free-stream velocity and is almost inversely proportional to $(Re_{\delta^*})_p$. In a favourable pressure gradient ($\beta = 1$) the ratio U_{TE}/U_e is not constant though it varies little in the direction of streaming. It is also not a constant in the present case. The range of $(Re_{\delta^*})_p$ considered when $\mathrm{d}p/\mathrm{d}x \neq 0$ was too small for a clear identification of the dependence of U_{TE}/U_e on $(Re_{\delta^*})_p$. One may state, however, that U_{TE}/U_e is larger when $\beta = 1$ than when $\beta = -0.1$, reflecting the effect of $\mathrm{d}p/\mathrm{d}x$ on the rates of elongation of the spot. The asymptotic celerity of the leading interface on the plane of symmetry of the spot is approximately $0.9U_e$, regardless of β, the type of disturbance, and $(Re_{\delta^*})_p$. The variation of U_{LE}/U_e with distance from the perturbation

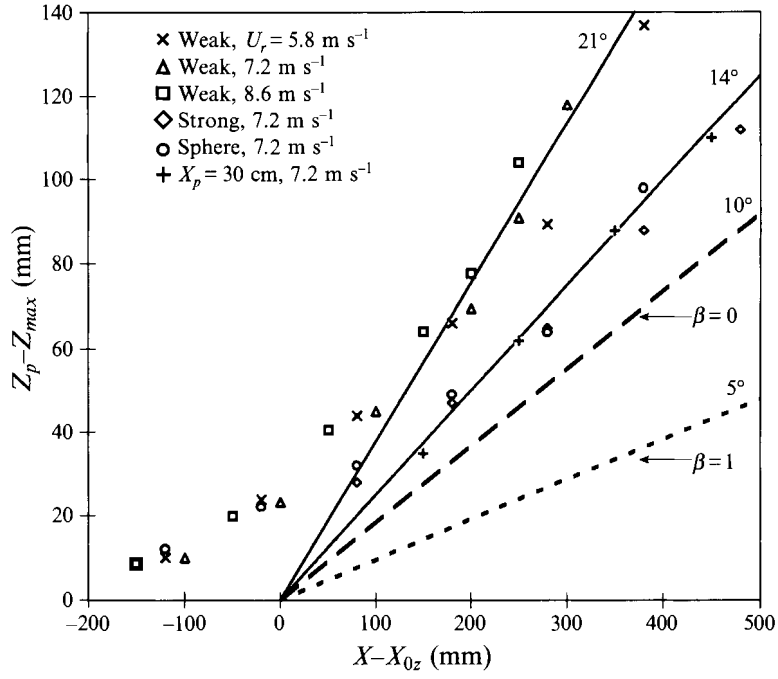

FIGURE 7. Spanwise spreading rates of spots at various pressure gradients. X_p = 50 cm, $\beta = -0.1$.

is plotted in figure 6(*b*) for $\beta = -0.1$. It is interesting to note that the variation of U_{LE}/U_e with X is almost the same for $\beta = -0.1$ and for $\beta = 1$ (Katz *et al.* 1990).

The spanwise rate of spread of the spot expressed as the angle measured at its virtual origin between its tip and its plane of symmetry is roughly 10° in the absence of a pressure gradient, regardless of $(Re_{\delta^*})_p$. This angle shrank to 5° when $\beta = 1$. The asymptotic lateral spreading angle measured for a weak impulsive disturbance is 21° (figure 7). The spanwise rate of spread of the spot is more sensitive to the pressure gradient and to the strength and duration of the initial disturbance than its elongation rate is. This rate of spread is more directly related to the mechanism by which the undisturbed surrounding boundary layer is being destabilized, as was discussed in some detail by Wygnanski *et al.* (1979) and Glezer *et al.* (1989). The secondary nonlinear instability causing the lateral spread of the spot is induced, perhaps, by the Λ-shaped vortices observed near its tip (Wygnanski 1981, 1983; Seifert *et al.* 1994). Spots generated by a strong disturbance, or a turbulent wedge triggered by a three-dimensional roughness, do not spread laterally at 21° but rather at 14° (figure 7). Strong streamwise vortices, created by the steady protuberance or by the long duration of the imposed disturbance, inhibit the natural destabilization process, making the spot narrower. Little is known about how the duration and strength of the disturbance affect the evolution of the spot. It was earlier concluded (Wygnanski *et al.* 1967), on the basis of measurements carried out on the plane of symmetry, that the asymptotic characteristics of the spot are independent of the disturbances generating it. The virtual origin X_{0z} used in figure 7 depends on the strength and duration of the perturbation. For the impulsive jet, X_{0z} is close to the location of the perturbation X_p but, for the weak perturbation generated by the hearing aid, it may occur as far as 300 mm downstream of X_p. Gostelow *et al.* (1993) followed the development of a spot in a more moderate adverse pressure gradient ($\beta = -0.052$) but their criteria for detecting its

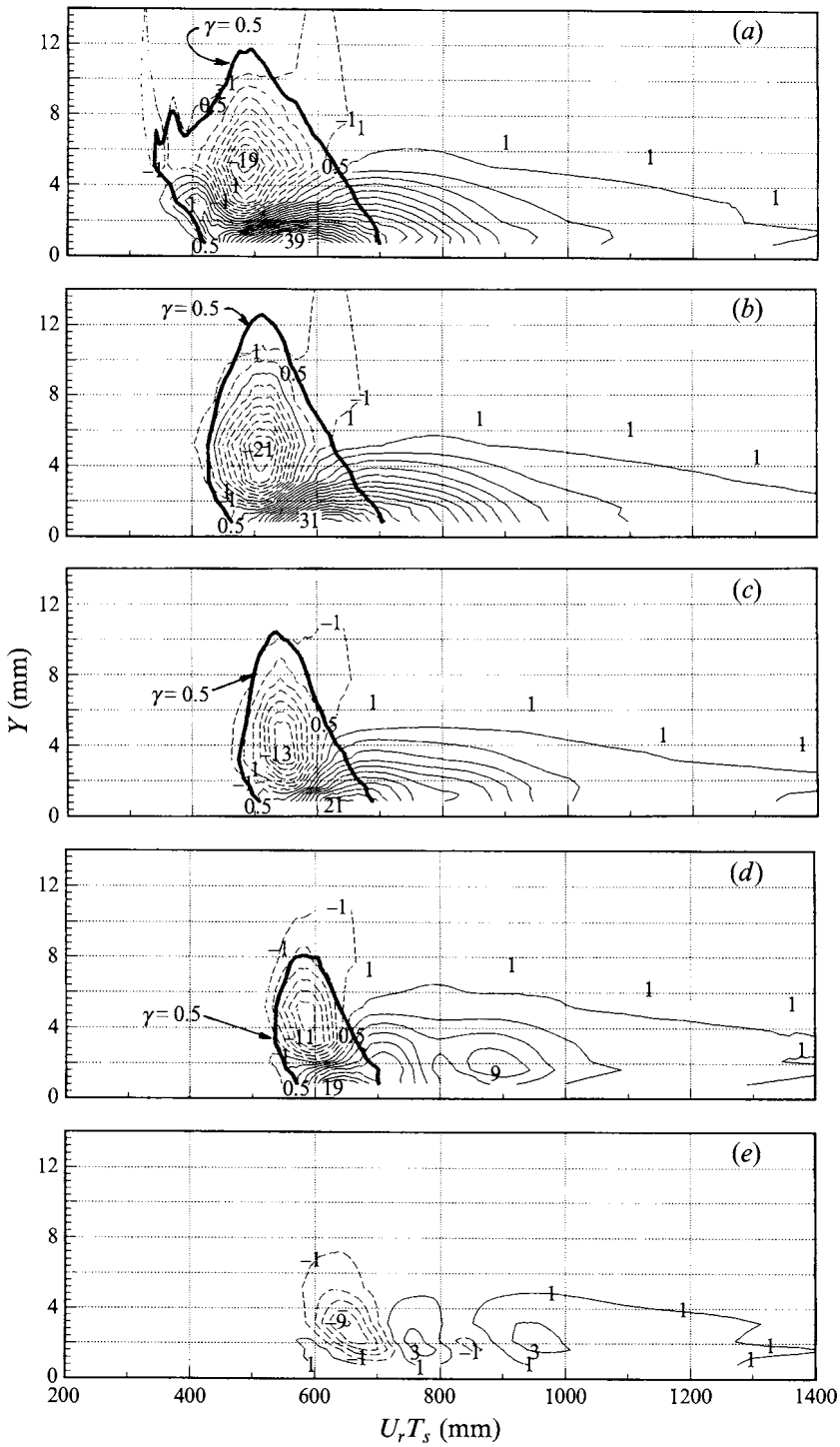

FIGURE 8. Velocity perturbation contours (plotted at 2% intervals) in the (Y, T)-plane due to spot passage. $X_p = 50$, $Z_p = 4$ cm, $X = 80$ cm, $U_r = 8.6$ m s^{-1}. (*a*) $Z_p - Z = 0$, (*b*) $Z_p - Z = 10$ mm, (*c*) $Z_p - Z = 20$ mm, (*d*) $Z_p - Z = 30$ mm, (*e*) $Z_p - Z = 45$ mm.

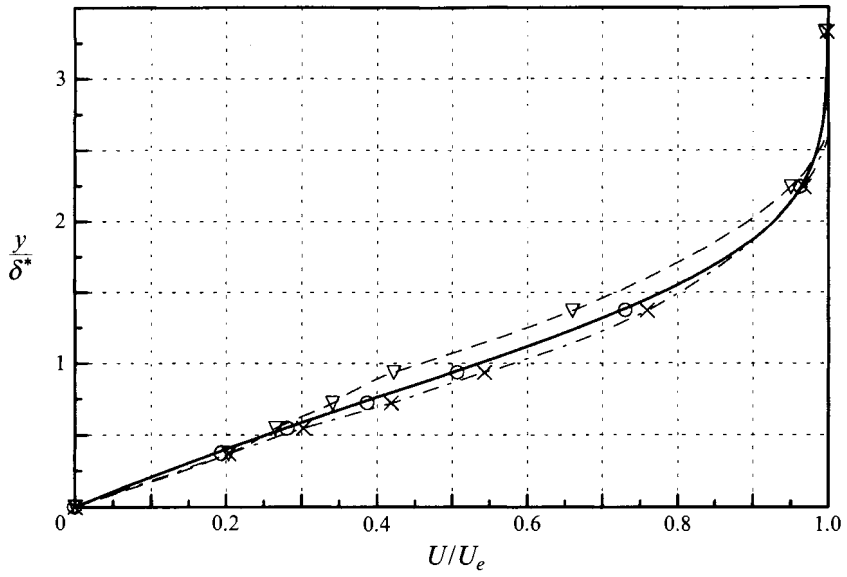

FIGURE 9. Ensemble-averaged velocity profiles corresponding to $Z_p - Z = 45$ mm, $X = 80$ cm, $Z = -5$ mm, $X_p = 50$, $Z_p = 4$ cm, and $U_r T_s = 200$ (○), 650 (▽) and 750 (×) mm (see figure 8*e*). ——, $\beta = -0.1$.

boundaries were based on the local shape factor, $H = \delta^*/\theta$, of the ensemble-averaged velocity profile. They reported that the lateral spreading angle between the spot tip and the plane of symmetry was 20°. Waves dominated the region near the tip up to an angle of 29°. The spanwise rate of spread of the spot was independent of $(Re_{\delta^*})_p$, as was the rate of its elongation along its plane of symmetry. However, the spanwise virtual origin of the spot depends on $(Re_{\delta^*})_p$ through its strong dependence on the free-stream velocity and a weak dependence on the location of the perturbation. Consequently, the location of this virtual origin does not scale with $(Re_{\delta^*})_p$ in a simple manner.

3.3. *The interaction between the spot and the waves*

The ensemble-averaged velocity perturbations and spot borders in the (Y, T)-plane are shown in figure 8. These plots correspond to the arrows marked on the (Z, T)-plane on figure 10(*c*). At this location ($X = 80$ cm) and reference velocity ($U_r = 8.6$ m s^{-1}), the displacement thickness of the laminar boundary layer is 2.3 mm. The perturbation contours corresponding to the plane of symmetry (figure 8*a*) have a very familiar form (e.g. see figure 16 in Wygnanski *et al.* 1982), with the maximum velocity defect situated directly underneath the summit of the spot. At exactly the same time, the region marked by the velocity excess near the surface is squeezed downward, and it extends only to 17% of the spot's height. The maximum defect of velocity on the plane of symmetry is −20% and is similar to observations made in the absence of a pressure gradient. The maximum excess of velocity in this case is 39%, which is much higher than is customary in the absence of $\mathrm{d}p/\mathrm{d}x$. The strong excess of velocity near the surface (see also figure 14) is associated with $\mathrm{d}p/\mathrm{d}x > 0$, which also results in a strong generation of waves. Their breakdown might have increased the excess velocity perturbation within the spot. The strength of both velocity perturbations diminishes with increasing spanwise location, but the ratio between the maximum velocity defect and excess is approximately constant. The velocity-excess perturbation disappears from the front of the spot at $Z - Z_p = 10$ mm, but it reappears again in the mean at

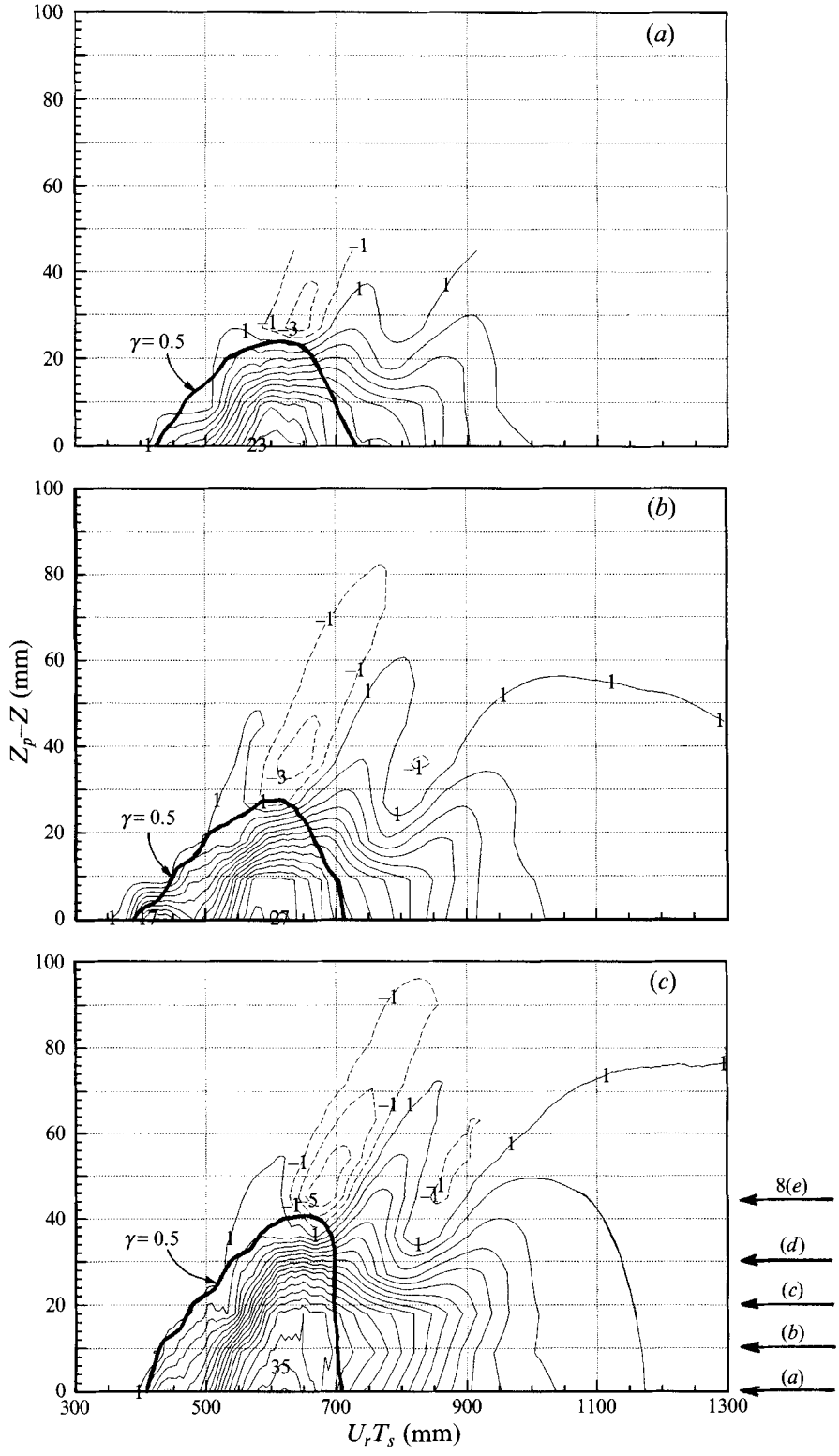

FIGURE 10. The effect of the reference velocity on the ensemble-averaged perturbation velocity contours in the (Z, T)-plane near the surface. $X_p = 50$, $Z_p = 4$ cm, $X = 80$ cm. (*a*) $U_r = 5.8$ m s^{-1}, (*b*) $U_r = 7.2$ m s^{-1}, (*c*) $U_r = 8.6$ m s^{-1}.

$Z-Z_p = 30$ mm. This suggests that streaky structures or streamwise vortices might exist near the surface. Furthermore, at $Z-Z_p = 30$ mm, the velocity excess in the calmed region is wavy, showing distinct regions of local maxima. Beyond the tip of the spot (i.e. at $Z-Z_p = 45$ mm, see figure 8*e*), velocity perturbation contours of both signs are associated with the wave packet. These contours can provide a link between the velocity perturbations generated by finite-amplitude waves and the velocity distortions associated with the turbulent spot closer to the plane of symmetry. The strong spanwise gradient in the excess velocity near the surface inferred from figures 8(*e*) and 8(*d*) and from figure 10(*c*) suggests the existence of a strong vortex near the tip of the spot (one should remember that the spanwise distances in figure 10 are stretched by a factor of about 5).

Three ensemble-averaged velocity profiles measured outside the tip of the spot (i.e. at $Z-Z_p = 45$ mm) at times corresponding to $U_r T_s = 200$ (undisturbed), 650, and 750 mm on figure 8(*e*) are plotted on figure 9, along with the theoretical velocity profile for $\beta = -0.1$. These velocity profiles mark distortions possessing local inflection points, which are larger than the range of distortions observed due to the imposed pressure gradients tested in our laboratory (i.e. the velocity profiles plotted on figure 3 and corresponding to $-0.1 < \beta < 1$). One expects, therefore, the existence of very strong secondary instabilities in the vicinity of the spot's tip. Similar observations were made at $\beta = 0$, but the velocity defect was not as strong and the defect region did not extend as far beyond the tip of the spot. Nevertheless it was referred to by Glezer *et al.* (1989) as the 'wave generator'. The secondary instabilities near the tip might be exacerbated by the probable existence of a spanwise velocity component (Seifert *et al.* 1994) and may lead to a rapid spanwise contamination of the laminar boundary layer by turbulence. The velocity-defect region persists along the entire leading edge of the spot from its centreline to its tip and even beyond (figure 8). The excess-velocity region near the wall terminates at the tip of the spot. It was shown by Seifert (1995) that a vertical impulsive jet creates a strong velocity deficit in the boundary layer which evolves within 20–30 cm into a wave packet and may even deteriorate to a spot when the perturbation is strong. This might suggest that the negative velocity perturbation outside the tips of the spot generates the wave packets trailing along its sides. A similar proposition was made by Glezer *et al.* (1989) for a spot evolving at $\beta = 0$.

The effect of Reynolds number at $\beta = -0.1$ on the intensity and spanwise extent of the waves is shown in figure 10. The disturbance generating all the spots was weak, and the data were taken at $X-X_p = 30$ cm. The measurements were performed at a distance from the surface corresponding to a location where the velocity was 35% of the reference velocity. Thus, only the free-stream velocity was changed between the three data sets presented in figures 10(*a*), 10(*b*) and 10(*c*). The plots shown in figure 10(*b*, *c*) resemble qualitatively the data presented by Gostelow *et al.* (1993); in both experiments, the waves emanating from the spot have a span that is either equal to or larger than the span of the spot. The velocity defect associated with the wave located at the extension of the spot's tip approximately doubled by increasing $(Re_{\delta^*})_p$ from 750 to 915 (figures 10*a* and 10*c*). The spanwise extent of the wave, measured by a 1% perturbation contour, increased by 22% between $(Re_{\delta^*})_p = 840$ and 915 (figures 10*b* and 10*c*). The spanwise extent of the spot depends on $(Re_{\delta^*})_p$ (or on U_r) and, in the cases considered here, there is an increase of 74% in the span between the data shown in figures 10(*a*) and 10(*c*). A part of the difference in the spanwise extent of the spots could stem from different virtual source locations. The characteristic length of the spot $(T_{TE}-T_{LE})\,U_e$ on its plane of symmetry is hardly affected by the Reynolds number, while the respective length of its calmed region (i.e. the region of excess velocity trailing

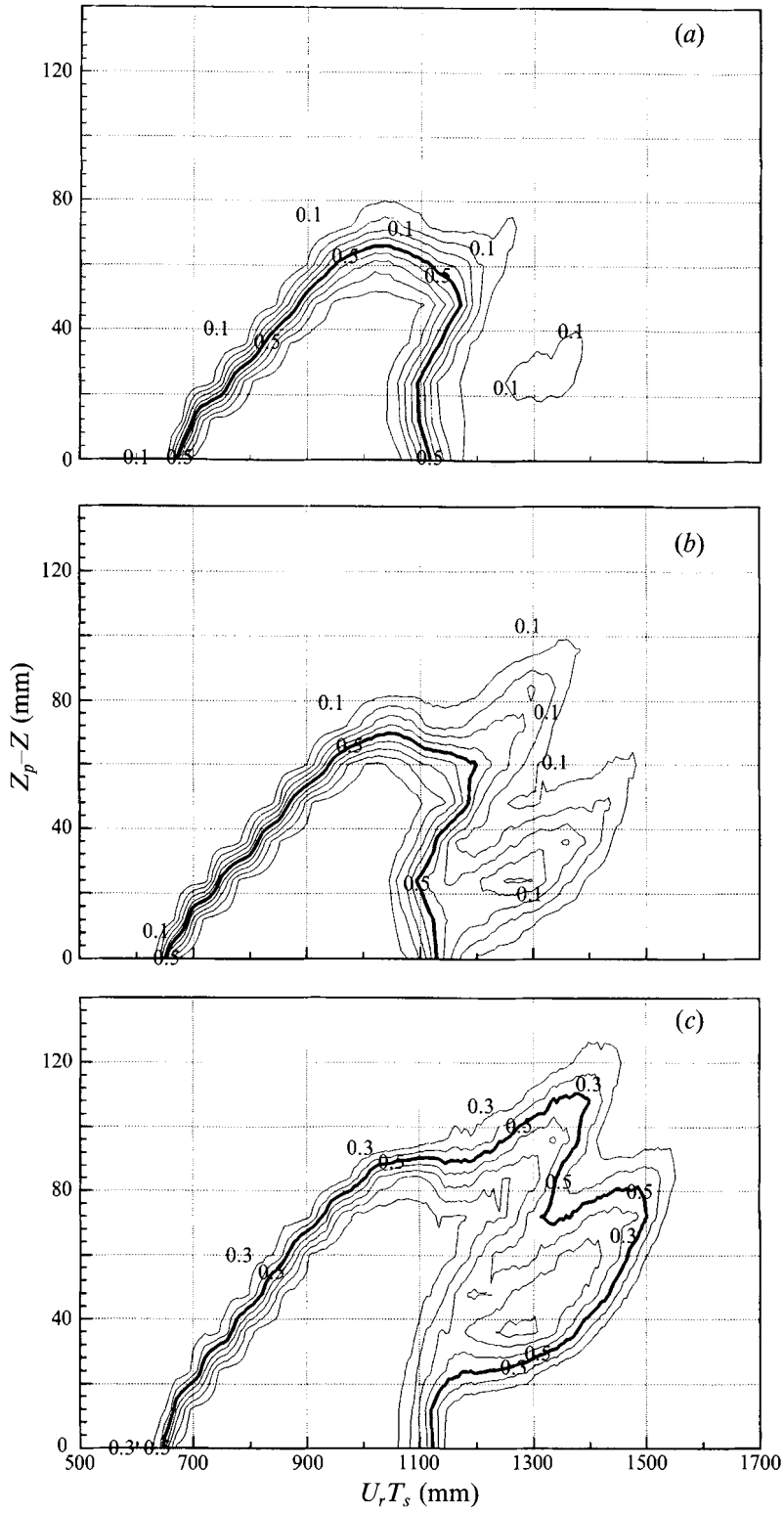

FIGURE 11. The effect of the reference velocity on the ensemble-averaged intermittency contours near the surface. $X_p = 50$, $Z_p = 4$ cm, $X = 100$ cm. (*a*) $U_r = 5.8$ m s^{-1}, (*b*) $U_r = 7.2$ m s^{-1}, (*c*) $U_r = 8.6$ m s^{-1}.

the spot) increases by a factor of 1.75 (figures 10*a* and 10*c*). This observation reinforces the notion that the calmed region is partly a by-product of the vortices induced by the initial disturbance and partly a product of the waves. In this context, the calmed region and the 'wave generator' represent a lasting nonlinear distortion of the mean flow. The duration of the calmed region might best be compared to the duration of the spot, provided the comparison is made in the same range of Reynolds numbers and distances from the origin. Such a comparison was made on the plane of symmetry, where the boundaries of the spot were determined on the basis of intermittency and the calmed region was assumed to be bounded between the spot's trailing edge and the 2% excess-velocity perturbation contour near the surface. A typical ratio between the duration of the calmed region and the turbulent spot was approximately 3, at a downstream distance of 500 mm from the source. It was approximately 2 in the absence of a pressure gradient and only 1 when $\beta = 1$. The relative duration of the calmed region appeared to be independent of the distance from the source and almost independent of the Reynolds number at $\beta = 0$ and 1, while it was increasing with this distance and Re in the present case.

Plan views of intermittency contours representing the variations in the shape of the spot near the surface (at a Y-location corresponding to $0.35 \times U_r$) are plotted in figure 11 (*a–c*) for three different reference velocities corresponding to $(Re_{\delta^*})_p = 750$, 840 and 915 at $X - X_p = 50$ cm. The measurements shown were taken at a single streamwise location 50 cm downstream of the perturbation produced by a pulsed earphone that generated fully developed spots 30 cm further downstream. The abscissa in this figure is proportional to the length of the spot as determined by the product of its duration and the reference velocity; the actual length on the plane of symmetry is approximately 350 mm. This length was obtained by assuming a representative convection velocity of $0.7U_e$, which produced a correct L_x at this X-station. At the lowest $(Re_{\delta^*})_p$, the spot has its familiar form with minor secondary breakdown of waves present behind its trailing edge. The closed intermittency contour of $\gamma = 0.1$, which is separated from the rest of the spot, represents this breakdown. At $(Re_{\delta^*})_p = 840$ (figure 11*b*), the average shape of the spot's boundary marked by $\gamma = 0.5$ is not much different from the one observed at lower $(Re_{\delta^*})_p$ and plotted in figure 11 (*a*) because the broken waves occurred in less than 50% of the events (there is a tiny region following the spot in which γ exceeds 50%). The intermittency contours following the spot's boundary mark the regions in which two wave crests associated with the spot consistently break down. These contours increase in value in the general direction of the plane of symmetry (see figure 10), suggesting that a more frequent breakdown occurs on the inboard part of the most upstream wave crests (i.e. the ones located farthest from the spot in the direction of streaming or, conversely, the ones that originated first near the tip region. The neighbouring crests, which are closer to the tips of the spots, have smaller amplitudes and thus break down less often. The value of $\gamma_{max.}$ along these crests is only 30% (figure 11*b*). By increasing $(Re_{\delta^*})_p$ to 915 (figure 11*c*) both wave crests broke down in more than 50% of the occurrences, thus distorting the ensemble-averaged boundary of the spot. The average trailing edge of the spot sweeps backward as a consequence of the additional breakdown. There are occurrences in which the waves break down before or perhaps even without joining the turbulent region of the primary spot, thus generating secondary spot-like structures, as was observed by Wygnanski *et al.* (1979) and Glezer *et al.* (1989) in the absence of a pressure gradient. A similar observation, based on the local minimum in γ between the main body of the original spot and the turbulent region created by the broken-down waves, can be made in the present study (figure 11*c*).

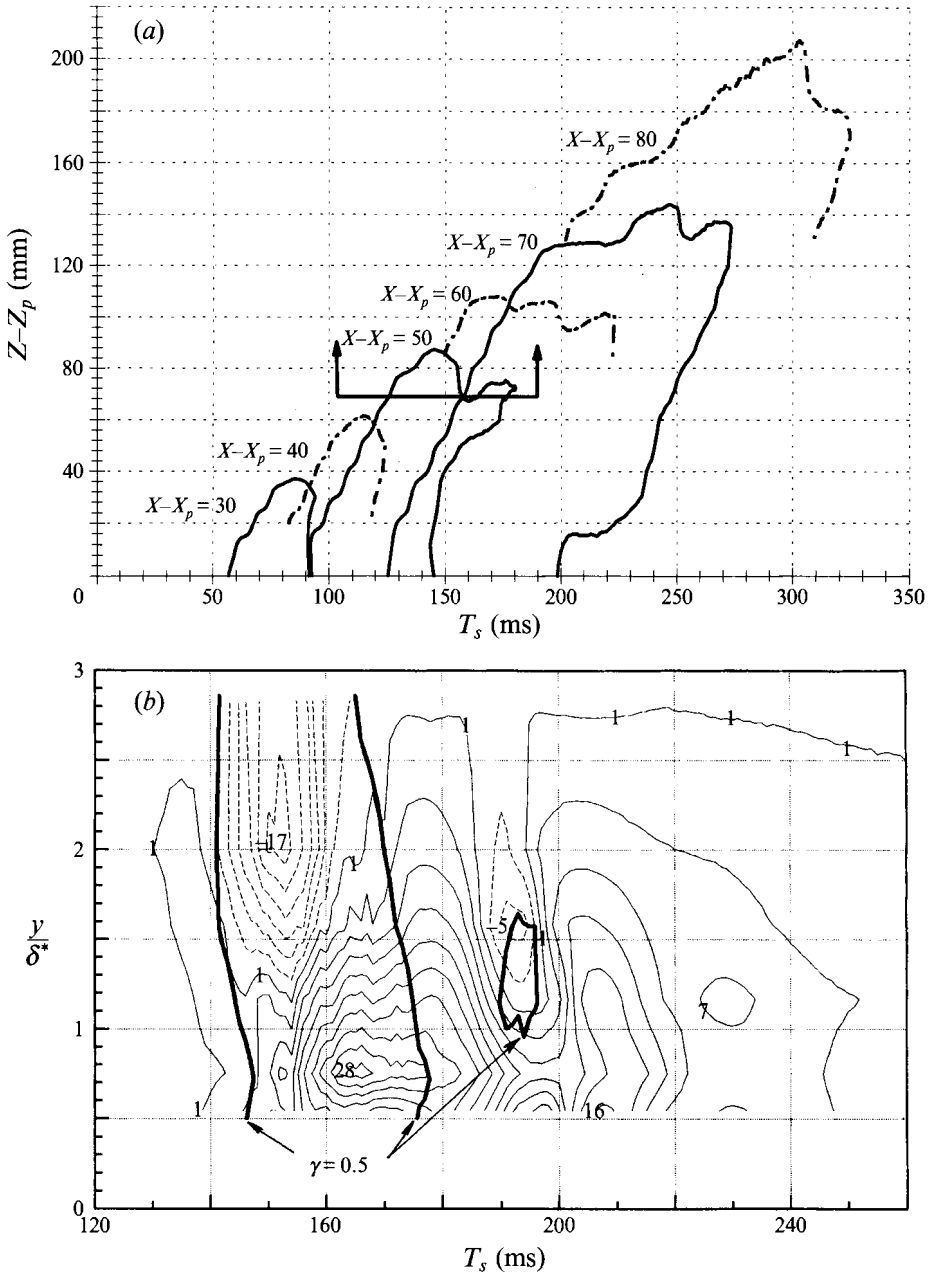

FIGURE 12 (*a*, *b*). For caption see facing page.

The evolution of the average spot boundary (contour level $\gamma = 0.5$) with X is plotted in figure 12(*a*). The perturbation was located in this case 30 cm downstream of the leading edge of the plate where $(Re_{\delta^*})_p = 650$, allowing one to follow the evolution of the spot over longer distances before the occurrence of a spontaneous transition that otherwise might have obscured the observations. The spanwise growth of the spot with increasing streamwise distance is obvious.

A significant distortion of the trailing interface of the spot attributable to the wave breakdown was observed for the first time at $X - X_p = 50$ cm (figure 12*a*). This

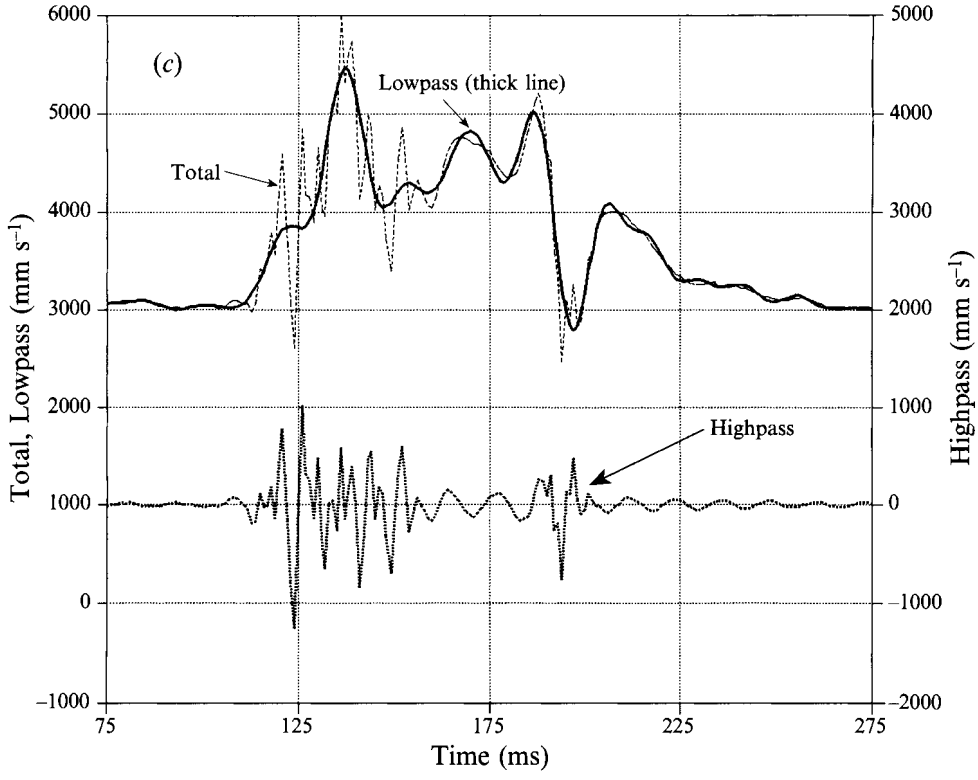

FIGURE 12. (*a*) Plan view of spot boundaries near the surface. $X_p = 30$, $Z_p = -5$ cm, $X = 100$ cm, $U_r = 7.2$ m s^{-1}. (*b*) Velocity perturbation contours showing a secondary breakdown (section marked by arrows in *a*). (*c*) Velocity of a single spot showing a secondary breakdown.

turbulent region increases in size by spreading toward the plane of symmetry with increasing X. An elevation view showing the velocity perturbation contours superimposed on the boundaries of the spot (i.e. contours of $\gamma = 0.5$) at this X-location and at $Z - Z_p = 7$ cm is plotted in figure 12(*b*). It indicates that the distortions of the spot's boundaries seen in figure 12(*a*) start when a separate turbulent region trailing the spot merges with it. It also indicates that the prevailing breakdown to turbulence occurs in the outer part of the surrounding boundary layer, as was first observed by Kovasznay, Komoda & Vasudeva (1962). The breakdown to turbulence is associated with the negative velocity perturbation generated by the wave packet and, thus, the bulk of the turbulent region inside the spot has a negative velocity perturbation, even on the plane of symmetry (e.g. see figure 8, and Wygnanski *et al.* 1982).

In order to be sure that the observations regarding breakdown are not an outcome of jitter associated with ensemble-averaging procedures, we examined numerous individual realizations. As an example, a temporal record of velocity taken at $Z - Z_p = 3.6$ cm is plotted in figure 12(*c*). It shows that the high-frequency fluctuations associated with the arrival of the turbulent spot are coupled with a general increase in velocity near the surface. Most of the perturbation velocity associated with the passage of the spot, and with the waves trailing it, is captured by low-pass filtering of the signal between 0 and 78 Hz. However, the high-pass-filtered signal above 80 Hz contains the turbulence and a fraction of the wave energy (figure 12*c*). The choice of 80 Hz as the dividing frequency was based on two criteria,

(i) the ensemble average of the low-pass-filtered signal would be identical to the ensemble average of the total signal, and

(ii) the ensemble average of the high-pass-filtered signal would vanish, but the results are not sensitive to the precise choice of the cut-off frequency. It is clear that the secondary breakdown occurs first in a separate region behind the spot, where the velocity defect is largest and that during the initial breakdown the velocity near the surface is not yet distorted. Initial breakdown to turbulence was often tied to a large-amplitude negative velocity perturbation, regardless of whether it occurred in a boundary layer (Klebanoff, Tidstrom & Sargent 1962) or in a pipe (Wygnanski, Sokolov & Friedman 1975). These observations represent the main features of the breakdown process, and they might assist in designing schemes for the actual delay of transition.

The effect of pressure gradient on the planform of the spot is shown in figure 13, where the velocity perturbation contours and the intermittency contour representing the location of the average spot boundary (i.e. $\gamma = 0.5$) are compared at $\beta = -0.1$, 0, and $+1.0$. Waves are observed at $\beta = -0.1$ and 0 (Seifert *et al.* 1994), but they are not seen at comparable Reynolds numbers at $\beta = 1.0$ (Katz *et al.* 1990). The wave packet seen in the presence of an adverse pressure gradient starts at the tip of the spot and is closely following its average trailing edge. The wave packet observed at $\beta = 0$ lags behind the spot, and there is a region of negative velocity perturbation near the tip of the spot. It is oriented in the streamwise direction when $\beta = 0$ and the waves seem to have emerged from it. It was thus called the 'wave-generator' by Glezer *et al.* (1989), and it was less stable than the rest of the surrounding boundary layer because the velocity profile measured in it contained an inflection point. Seifert *et al.* (1994) showed that inside the spot there is a very strong outwardly directed cross-flow in the tip region. This might contribute to the local instability of the flow in the 'generator' and the spanwise spreading rate of the spot. The wave packet that behaves in a conventional linear or weakly nonlinear manner may or may not interact with the spot depending on the Reynolds number of the surrounding boundary layer. In the present case (for $\beta = -0.1$), the negative perturbation region has the same orientation and scale as the waves whose presence in this region is very clear (see also figure 10). Nevertheless, the velocity perturbation near the spot's tip tends to be more negative than it is at a later time. No waves were observed at $\beta = 1.0$, because the wave generation near the spot's tip is associated with the stability of the surrounding boundary layer and the Reynolds number of the surrounding flow was much lower than $Re_{crit.}$. When Re is close to but lower than $Re_{crit.}$, waves are often generated and amplified near the tip, where the flow might be locally supercritical. (The condition for supercriticality is not actually required because there might be a transient growth due to the presence of the spanwise velocity component near the 'wave generator'; see Seifert *et al.* 1994.) The waves lagging the spot and emerging from the 'wave generator' might decay farther downstream unless the ambient flow becomes supercritical, permitting them to resume their amplification. In this manner, secondary breakdown occurs and with it the formation of a new turbulent region that either distorts the spot's trailing edge (figures 11 and 12*a*) or generates a small but distinctly separate spot (Wygnanski *et al.* 1979; Glezer *et al.* 1989). The different planforms of the spots shown in figure 13 reflect such a secondary breakdown.

3.4. *The effect of the initial disturbance on the evolution of the spot*

The spots in the present experiment were generated either by a small earphone or by a pneumatic valve connected to a high-pressure source. The strength and the duration

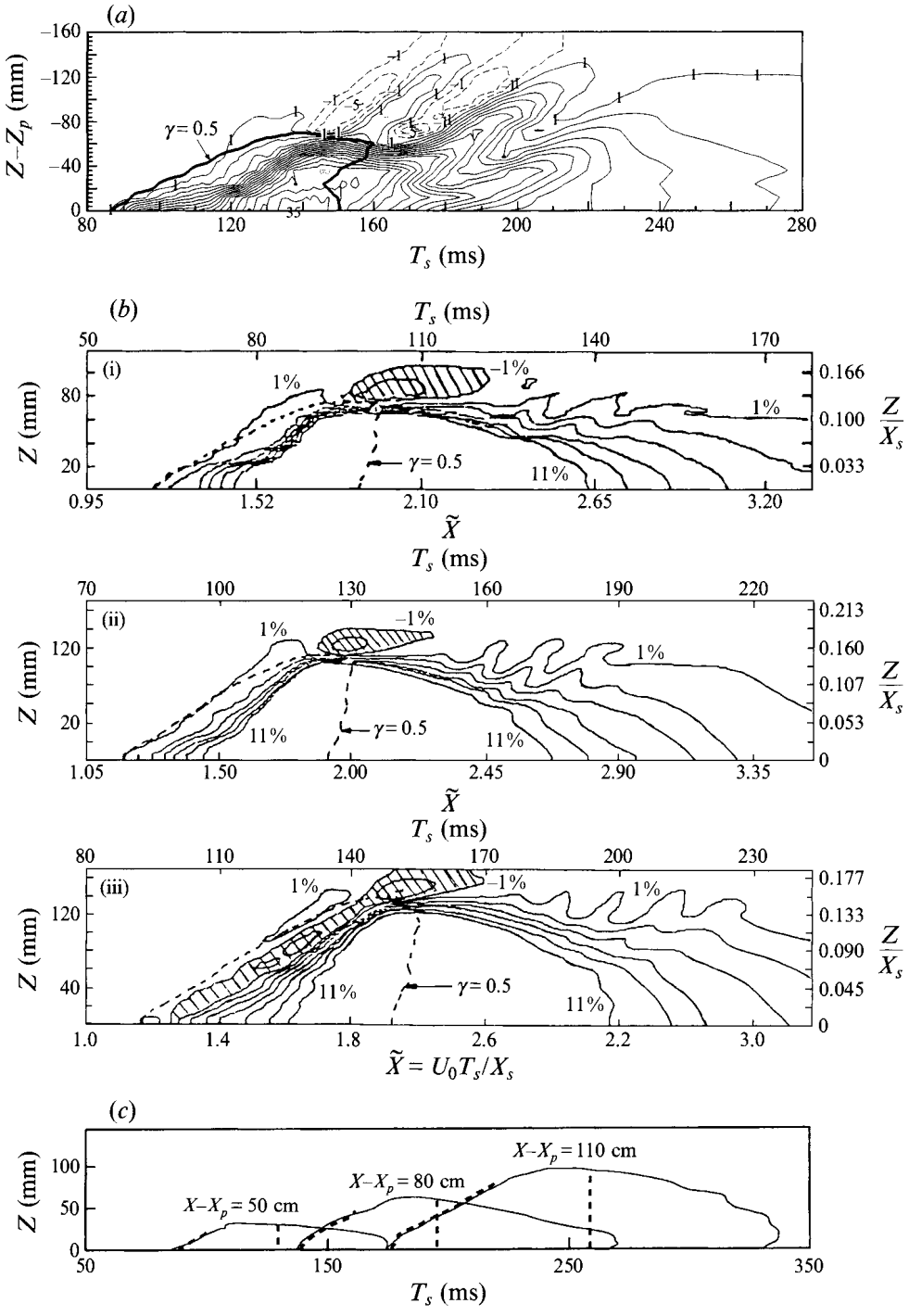

FIGURE 13. A comparison of the ensemble-averaged velocity perturbation and spot boundaries in the (Z, T)-plane ($X_p = 50$, $Z_p = 4$ cm, $X = 100$ cm, $U_r = 7.2$ m s^{-1}) at three pressure gradients corresponding to (*a*) $\beta = -0.1$; (*b*) $\beta = 0$ and (i) $X_s = 60$ cm, $y/\delta^* = 1.05$; (ii) $X_s = 75$ cm, $y/\delta^* = 1$, (iii) $X_s = 90$ cm, $y/\delta^* = 0.95$; (*c*) $\beta = 1$ and ---, $\gamma = 0.5$; ——, 2% U_{pert}.

of the two perturbations were quite different and it transpired that some of the differences in the characteristics of the spot stem from the different strengths of the disturbances. We shall try to identify and explain some of these differences.

It was observed that the initial length of a spot generated by a strong disturbance is longer than the corresponding length generated by a weak one; however, the asymptotic rate of elongation of a strong-disturbance spot is generally smaller. This observation may be explained by assuming that the disturbance is similar to a jet in a cross-flow. The stronger and longer disturbance generates a larger region of turbulence and, therefore, an initially larger spot. However, the jet in a cross-flow generates two counter-rotating streamwise vortices (resembling a mushroom in a cross-sectional view), which induce a downward stabilizing motion at their edges and inhibit the rate of destabilization of the boundary layer. In this case, the asymptotic rate of spread of the spot in both the spanwise and streamwise directions are diminished (see figure 7 and the discussion in §3.2). The slope, $\mathrm{d}(U_{TE}/U_e)/\mathrm{d}X$, may change sign, depending on the strength of the perturbation generating the spot. A strong perturbation results in $\mathrm{d}(U_{TE}/U_e)/\mathrm{d}X > 0$ and a smaller rate of elongation of the spot. The solid line in figure 6 separates the results due to the strong perturbation (above) and the weak one (below). This behaviour was not observed in previous investigations and requires further study. The asymptotic leading-edge velocity of the spot is about $0.9U_e$, regardless of U_r, and seems to be independent of the type of disturbance generating the spot.

The lateral propagation velocity of some recognizable features of the spot's tip initiated at $X_p = 30$ cm by a weak disturbance (presented in figure 12*a*) at large X, is approximately 0.7 m s^{-1}. This translates to a spreading angle of 14° because the spot's tip advances downstream at an approximate celerity of $C_x = 0.45U_e$ (figure 6). The lower spanwise spreading rate observed in this case corresponds to the spreading rates of spots generated by stronger disturbances at $X_p = 50$ cm (figure 7). This might have been caused by the weaker adverse pressure gradient prevailing near the perturbation (i.e. at $X_p = 30$ cm because only for $X > 50$ cm is the pressure gradient parameter $\beta = -0.1$; see figure 2).

The sensitivity of the spanwise rate of spread of the spot to the strength and duration of the initial disturbance (see §3.2) is correlated with its average shape and the velocity perturbations marking its passage. A plan view of these mean quantities near the surface (i.e. at Y corresponding to $0.35U_r$) is plotted in figure 14(*a*, *b*). Both spots originated at $X_p = 50$ cm and were mapped at $X = 100$ cm with the sole difference in the results stemming from the strength and duration of the perturbations. The planforms of the intermittency contours (only the contours of $\gamma = 0.2$ and 0.5 are plotted and marked by the heavy lines in figure 14) and of the velocity perturbation contours are quite different for the two cases considered. The average span of the spots generated by weak disturbances was 70 mm (figure 14*a*) while the span of the spots generated by impulsive jets (which represent a strong and a relatively long perturbation) was 110 mm, although their duration on the plane of symmetry was almost identical. Thus, the spanwise extent of the spot is sensitive to the disturbance generating it while its streamwise dimension on the plane of symmetry is not. This is consistent with the observations of Wygnanski *et al.* (1976), who suggested that the length and the structure of the spot on its plane of symmetry are independent of its origin. Wygnanski *et al.* did not investigate the effects of the different disturbances on the spanwise evolution of their spots. The duration of the calmed region is also quite different between figures 14(*a*) and 14(*b*), if one defines the boundary of the calmed region by a positive velocity perturbation $(U - U_{lam})/U_e = 2\%$. In one case, it terminates at $T_s = 300$ ms and in the other it terminates at $T_s = 380$ ms and is not even presented

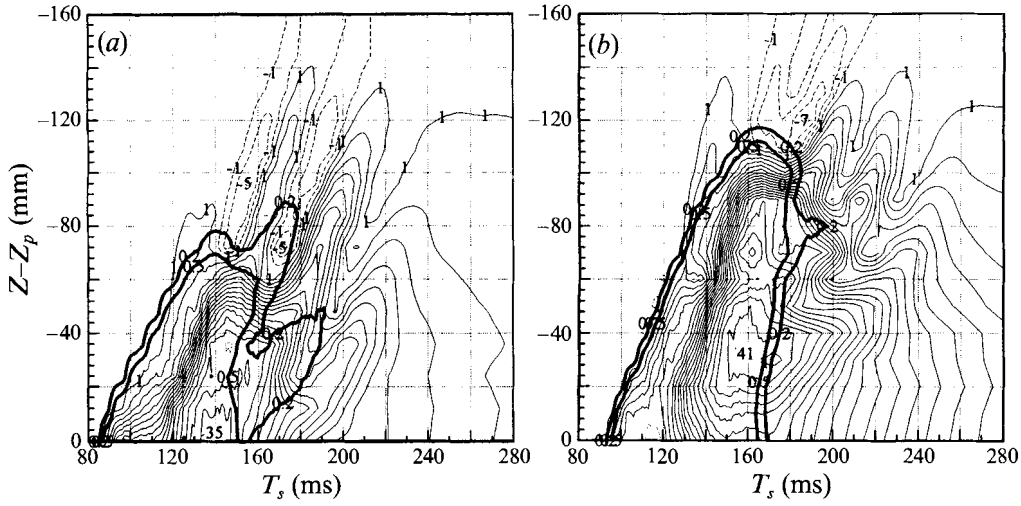

FIGURE 14. The effect of the disturbance strength on the spot boundaries and velocity perturbation contours. $X_p = 50$, $Z_p = 4$ cm, $X = 100$ cm $U_r = 7.2$ m s^{-1}. (*a*) Weak disturbance, (*b*) strong disturbance.

on the figure. Therefore, the duration of the calmed region may scale better with the spanwise extent of the spot than with its streamwise length and possibly with the strength of the perturbation initiating the spot.

The maximum spanwise extents of the wave packets, observed beyond the extremities of the average spot's boundaries, were almost identical in figures 14(*a*) and 14(*b*) (i.e. independent of the strength of the perturbation generating the spot and thus independent of the location of the boundaries of the spot). The maximum velocity perturbation, $(U-U_{lam})/U_e$ occurs inside the spot near its trailing interface. It is equal to 0.35 when the perturbation is weak and 0.41 when it is strong. It is interesting to note that, in the latter case, the maximum velocity perturbation contours are not located on the plane of symmetry of the spot (as they are for the weak perturbation) but rather at 30% of its span. At the same spanwise location, the wave crest (marked by a negative perturbation in the u-component) farthest from the spot boundary (i.e. the most upstream wave detectable) turns in the direction of streaming. The two occurrences seem to be related, as was already observed by Glezer *et al.* (1989) (their figure 14) in the absence of a pressure gradient. The neighbouring wave crest downstream also turns in the streamwise direction where another maximum of the velocity perturbation occurs inside the spot. This maximum is located at 50% of the span in the weak-perturbation case and at 65% of the span for the impulsive jet. The intermittency factor of 20% (i.e. the contour along which $\gamma = 0.2$, which is marked by a heavy line on figure 14) follows the minima of the velocity perturbations (i.e. the wave crests) and also increases along them, suggesting that a partial breakdown of these waves occurs where the velocity perturbation has a local minimum (see also figure 12*c*) and eventually distorts the average shape of the spot. The delay of wave breakdown behind the trailing edge of the spot generated by an impulsive jet might be associated with a longer more intense calmed region. The distortions in the spot's trailing edge might also be coupled to the duration of the calmed region and to the strength of the waves at the tip. Another interesting observation is that the maximum velocity defect outside the spot is higher for the impulsive jet spot (-7% in figure 14*b*) than for the spot generated by the hearing aid (-5% in figure 14*a*).

4. Conclusions

The rate of growth of a turbulent spot in a laminar boundary layer is enhanced by an adverse pressure gradient when all other parameters affecting the spot are kept constant. Therefore, small differences in the normalized shape of the undisturbed velocity profile might have a major effect on the transition of the laminar boundary layer. It also appears that the adverse pressure gradient affects the sensitivity of the boundary layer to the strength and the duration of the disturbances generating the spot. A weak disturbance generated spots whose tips spread in the spanwise direction at half an included angle of 21° compared to a typical angle of 10° measured with $\beta = 0$. A stronger disturbance reduced the asymptotic rate of spread of the spot. This finding was correlated with the strength and duration of the 'calmed region' trailing the spot, which was also affected by the intensity of the disturbance. The normalized length of the calmed region relative to the length of the spot is much greater for $\beta = -0.1$ than for $\beta = 0$. The calmed region might therefore scale with the span of the spot rather than its length. This feature might not only help us to understand the breakdown process but perhaps even control it by periodically generating spots across the entire span of the boundary layer (Seifert 1995). The interaction of the spot with the wave packet trailing it is also enhanced by the adverse pressure gradient because the Reynolds number of the surrounding flow is almost everywhere supercritical.

Since the presence of the adverse pressure gradient enhances the interaction between wave packets (whose behaviour can be predicted by using stability analysis) and the spot (whose characteristics we know only from experiment), one may study the breakdown process in this configuration. Similar studies in the absence of a pressure gradient were inconclusive, partly because the interaction with the waves was peripheral to the evolution of the spot and partly because of difficulties with instrumentation. We have thus acquired a digital particle image velocimeter, which will give us instantaneous information about the entire cross-section of the spot. Such information, coupled with direct Navier–Stokes simulation, may shed more light on the transition process and on the ways to control it. We believe that the spot evolving in an adverse pressure gradient is most suitable for this endeavour.

The authors would like to thank Mr B. Margaliot for his assistance in adjusting and measuring the base flow and Mr Y. Mytnik and Mr D. Heifetz for their assistance in gathering, processing, and presenting the data.

REFERENCES

CANTWELL, B., COLES, D. & DIMOTAKIS, P. 1978 Structure and entrainment in the plane of symmetry of a turbulent spot. *J. Fluid Mech.* **87**, 641.

CHAMBERS, F. W. & THOMAS, A. S. W. 1983 Turbulent spots, wave packets and growth. *Phys. Fluids* **26**, 1160.

EMMONS, H. W. 1951 The laminar turbulent transition in a boundary layer-part I. *J. Aero. Sci.* **18**, 490.

GAD-EL-HAK, M., BLACKWELDER, R. F. & RILEY, J. J. 1981 On the growth of turbulent regions in laminar boundary layers. *J. Fluid Mech.* **110**, 73.

GLEZER, A., KATZ, Y. & WYGNANSKI, I. 1989 On the breakdown of the wave packet trailing a turbulent spot in a laminar boundary layer. *J. Fluid Mech.* **198**, 1.

GOSTELOW, J. P. 1993 Some scenarios for transition on turbomachinery blading. Paper Presented at the *End stage transition Conf., Syracuse University.*

GOSTELOW, J. P., HONG, G., MELWANI, N. & WALKER, G. J. 1993 Turbulent spot development under a moderate pressure gradient. *ASME Paper* 93-GT-377.

KATZ, Y., SEIFERT, A. & WYGNANSKI, I. 1990 On the evolution of a turbulent spot in a laminar boundary layer in favorable pressure gradient. *J. Fluid Mech.* **221**, 1.

KLEBANOFF, P. S., TIDSTROM, K. D. & SARGENT, L. M. 1962 The 3D nature of boundary layer instability. *J. Fluid Mech.* **12**, 1.

KOVASZNAY, L. S., KOMODA, H. & VASUDEVA, B. R. 1962 Detailed flow field in transition. In *Proc. 1962 Heat Transfer and Fluid Mech. Inst., Palo Alto, CA*, p 1. Stanford University Press.

MORKOVIN, M. V. 1969 On the many faces of transition. In *Viscous Drag Reduction* (ed. C. S. Wells), p. 1. Plenum.

NARASIMHA, R. 1985 The laminar turbulent transition zone in the boundary layer. *Prog. Aerospace Sci.* **22**, 29.

SARIC, W. S. 1994 Görtler vortices. *Ann. Rev. Fluid Mech.* **26**, 379.

SCHUBAUER, G. B. & KLEBANOFF, P. S. 1956 Contributions to the mechanics of boundary layer transition. *NACA Rep.* 1289.

SEIFERT, A. 1990 On the interaction of low amplitude disturbances emanating from discrete points in a Blasius boundary layer. PhD thesis, Tel-Aviv University.

SEIFERT, A. 1995 To be published.

SEIFERT, A., ZILBERMAN, M. & WYGNANSKI, I. 1994 On the simultaneous measurements of two velocity components in the turbulent spot. *J. Engng Maths* **28**, 43.

WAZZAN, A. R., OKAMORA, T. T. & SMITH, A. M. O. 1968 Spatial and temporal stability charts for the Falkner–Skan velocity profiles. *McDonnel Douglas Corp. Rep.* DAC 67086.

WYGNANSKI, I. 1981 The effects of Reynolds number and pressure gradients on the transitional spot in a laminar boundary layer. In Lecture Notes in Physics, vol. **136**, p. 304. Springer.

WYGNANSKI, I. 1983 On turbulent spots. In *Proc. the 7th Biennial Symp. on Turbulence, Rolla, Missouri* (ed. G. K. Patterson & J. L. Zakin) p. 390.

WYGNANSKI, I., HARITONIDIS, J. H. & KAPLAN, R. E. 1979 On a Tollmien–Schlichting wave packet produced by a turbulent spot. *J. Fluid Mech.* **92**, 505.

WYGNANSKI, I. J., SOKOLOV, M. & FRIEDMAN, D. 1975 On transition in a pipe. Part 2. The equilibrium puff. *J. Fluid Mech.* **69**, 283.

WYGNANSKI, I., SOKOLOV, M. & FRIEDMAN, D. 1976 On a turbulent spot in a laminar boundary layer. *J. Fluid Mech.* **78**, 785.

WYGNANSKI, I., ZILBERMAN, M. & HARITONIDIS, J. H. 1982 On the spreading of a turbulent spot in the absence of a pressure gradient. *J. Fluid Mech.* **123**, 69.